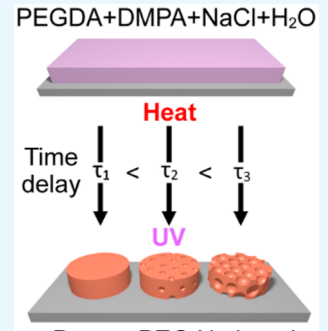
Cite This: ACS Appl. Mater. Interfaces XXXX, XXX, XXX–XXX

Sen Wang,[†] Le Li,[‡] Deanyone Su,[§] Kevin Robin,^{||} and Keith A. Brown*,[†],[‡],[‡],[‡]

Supporting Information

ABSTRACT: Independent control over phase separation and photo-cross-linking allows the structure and porosity of hydrogels to be patterned in a single photolithographic step. This observation is based upon a temperature-triggered spinodal decomposition of a ternary mixture of water, salt, and polymer into a salt-rich aqueous phase and a polymer-rich phase. Importantly, subsequent exposure to light arrests the phase separation, allowing the porosity state to be frozen in a cross-linked hydrogel network. Tuning the delay between the application of heat and illumination allows the pore size to be tuned between 400 nm and 4 μ m. By utilizing gray-scale photomasks, a single process can be used to define regions of pure hydrogel, porous hydrogel with a programmed average pore size, and blank substrate with no hydrogel. In addition to representing a combination of top-down and bottom-up processes that enables the realization of complex samples, the simplicity of this process and the versatility of the resultant patterns could provide a useful capability for the definition of hydrogel samples for the development of advanced biomaterials.



Porous PEG Hydrogel

KEYWORDS: hydrogels, photolithography, porosity, phase separation, tissue engineering

■ INTRODUCTION

Downloaded via BOSTON UNIV on September 27, 2018 at 12:53:49 (UTC). See https://pubs.acs.org/sharingguidelines for options on how to legitimately share published articles.

Biological tissue is a remarkably complex heterogeneous material with distinct structural features that span the nanometer to centimeter scales. 1-5 While structural control approaching this level is possible in the context of state-of-theart integrated circuits, 6 it is not yet possible to process soft materials with the requisite precision and throughput needed to recapitulate macroscopic biological tissue with control over every hierarchical scale. Hydrogels, or networks of hydrophilic polymers, are a leading material for tissue engineering due to their biocompatibility and processability.^{2,7} While patterning in aqueous environments introduces challenges not normally encountered in lithography for semiconductor processing, there have been remarkable advances in preparing hydrogel structures with high degrees of control. In addition to examples of patterning two-dimensional arrangements of hydrogels using photolithography,^{7,8} direct write additive manufacturing allows the structure of hydrogels to be tuned in three dimensions, albeit with a trade-off in throughput. 1,9 Additionally, photolithography has been adapted to pattern hydrogels with spatial control over their stiffness.3 While these approaches allow hydrogels to be patterned on the microscopic scale, controlling local porosity remains a major challenge. 10 Interestingly, there exist many approaches for preparing bulk hydrogel samples with known porosity, and these generally occur by introducing a porogen or a sacrificial material that holds the place of a pore while the hydrogel is cross-linked around it. 11 A critical feature

for porogens is that they have to be removable after crosslinking, which has led to the study of immiscible liquids, 12 ice, 13,14 air bubbles, 15 and notably salt crystals, 16 all of which can be removed post synthetically in a process known as leaching. Despite progress in the development of porogens, there is currently no way of scalably patterning the size and density of pores in a hydrogel. This synthetic roadblock is particularly important in the development of biomaterials for tissue engineering as pore size has been recognized as an important factor in determining how cells adhere, proliferate, differentiate, and excrete matrix-forming proteins. 17-20

In this manuscript, we explore how coordinating phase separation and cross-linking can lead to the scalable production of hydrogels with patterned porosity. While it is well established that hydrogels can be prepared through photocross-linking and that salt crystals present during cross-linking can form pores in hydrogels, we explore the hypothesis that heating a mixture of un-cross-linked polymer, salt, and water can lead to the formation of pores with locally controlled sizes (Figure 1). We begin by exploring the thermodynamics of mixtures of liquid poly(ethylene glycol) diacrylate (PEGDA), sodium chloride as a model salt, and water. This ternary system is governed by a rich phase diagram with a highly temperature-

Received: July 10, 2018 Accepted: September 12, 2018 Published: September 12, 2018

[†]Division of Materials Science & Engineering, Boston University, Boston, Massachusetts 02215, United States

[‡]Department of Mechanical Engineering, Boston University, Boston, Massachusetts 02215, United States

[§]Department of Electrical and Computer Engineering, Carnegie Mellon University, Pittsburgh, Pennsylvania 15213, United States

Edward M. Kennedy Academy for Health Careers, Boston, Massachusetts 02115, United States

¹Physics Department, Boston University, Boston, Massachusetts 02215, United States

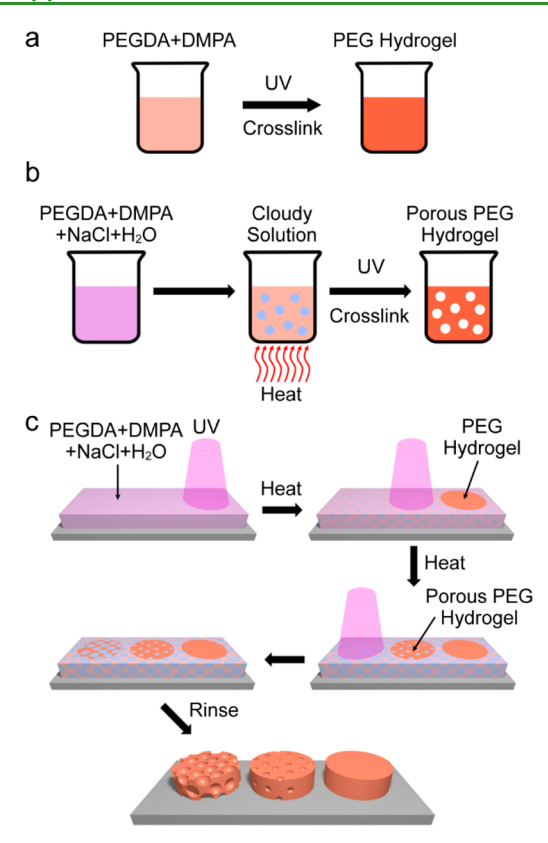


Figure 1. Patterning porosity by arresting phase separation. (a) Process of making pure poly(ethylene glycol) (PEG) hydrogels by photo-cross-linking poly(ethylene glycol) diacrylate (PEGDA) with the photoinitiator 2,2-dimethoxy-2-phenylacetophenone (DMPA). (b) Process of making porous PEG hydrogels through the heat-induced phase separation of a solution of PEGDA, DMPA, NaCl, and water. (c) Lithographic process for controlling the position and porosity of PEG hydrogels. By exposing a sample to UV light at different times during the phase separation process, the phase separation can be arrested leading to pores of well-defined size.

sensitive boundary between a single-liquid and two-liquid domain that we hypothesize can be exploited to phase separate in a useful manner in the context of lithography. Specifically, if the mixture includes a photo-cross-linker and is exposed to light, PEGDA cross-links to form a poly(ethylene glycol) (PEG) hydrogel that resists further phase separation. In order to explore this phenomena, we perform a series of experiments in which we prepare thin films out of a mixture of PEGDA, water, and salt, heat the films to begin phase separation, and subsequently expose them to light to arrest the phase separation process resulting in pores in the PEG hydrogel that can be tuned between 400 nm and 4 μ m. We further exploit this phenomenon by locally modulating light intensity using bright-field and dark-field photomasks to realize hydrogel films with porous domains and isolated hydrogel features with controlled porosity, respectively. Finally, we find that greyscale photomasks combine these attributes and allow one to pattern regions of controlled pore size, regions of pure hydrogel, and domains that are un-cross-linked, all in one step. Collectively, these advances allow for PEG films to be synthesized with control over their macroscopic structure and the size of their pores in a spatially dependent manner.

RESULTS AND DISCUSSION

In order to explore whether phase transitions of polymer solutions can be leveraged to control hydrogel porosity, we first experimentally determined the ternary phase diagram of mixtures containing PEGDA, water, and salt (Figure 2a). To

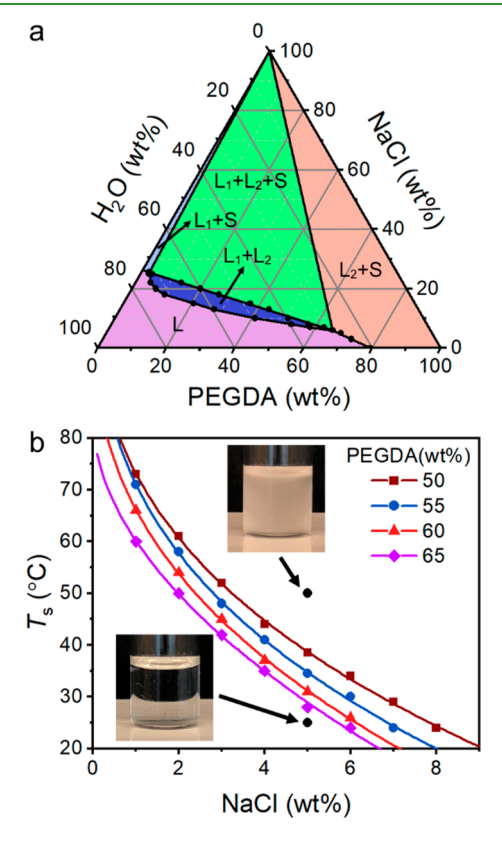


Figure 2. Phase behavior of mixtures of hydrophilic polymers, water, and salt. (a) Ternary phase diagram showing the equilibrium phases of PEGDA, $\rm H_2O$, and NaCl at 23 °C. At low salt concentrations, all three components form a single liquid phase (L). At higher salt concentrations, a salt-rich liquid ($\rm L_1$) and a PEGDA-rich liquid ($\rm L_2$) are stable. Further increasing the salt concentration leads to the precipitation of solid salt (S). (b) Spinodal temperature $T_{\rm s}$ at which a composition prepared in the region L decomposes into $\rm L_1$ and $\rm L_2$. Insets are photographs of pure L at low temperature and emulsions of $\rm L_1$ and $\rm L_2$ at an elevated temperature. Inset photographs show solutions prepared with 60% PEGDA by weight and held at T=25 °C (lower image, $T<T_{\rm S}$) or T=50 °C (upper image, $T>T_{\rm S}$).

determine the boundaries between phases, 700 Da PEGDA was titrated into mixtures of NaCl and DI water at room temperature (23 °C) until a transition was observed. At low salt concentrations, water and PEGDA are completely miscible giving rise to a single liquid phase (L). At higher salt concentrations, the mixture becomes an emulsion of a salt-rich liquid (L₁) and PEGDA-rich liquid (L₂), due to the limited solubility of salt in PEGDA. Further increasing the salt concentration leads to the precipitation of solid salt (S). This general behavior is similar to the phase behavior of ternary mixtures of glycerol, water, and salt.²¹ In order to exploit this equilibrium phase diagram to create porous hydrogels, one could operate in region L2+S, where PEGDA-rich L2 coexists with salt crystals.²² If a mixture with this composition is exposed to UV light, the PEGDA can cross-link around the salt crystals. Subsequent rinsing with water can be used to remove

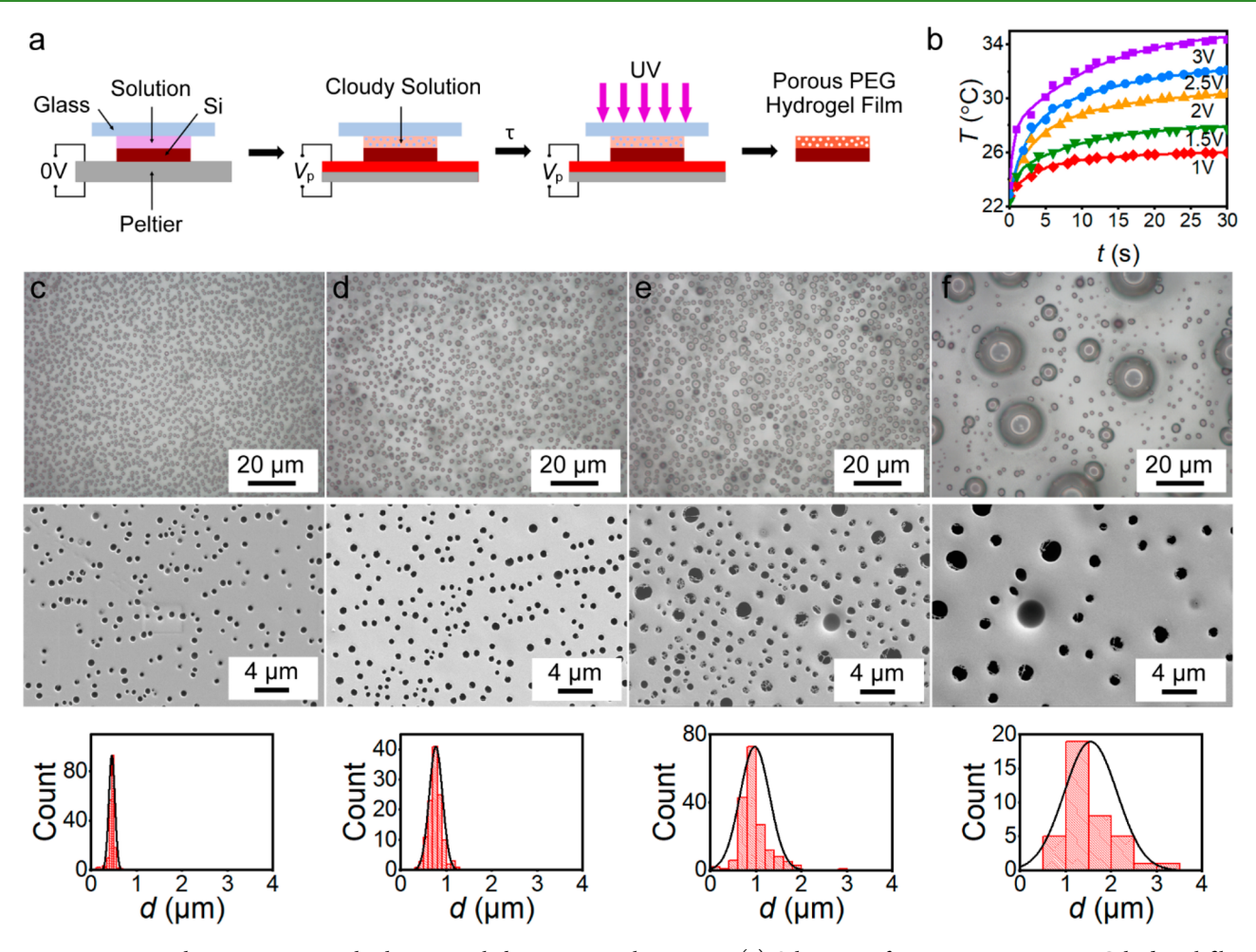


Figure 3. Arresting phase separation with photo-cross-linking to control pore size. (a) Schematic of preparing a porous PEG hydrogel film. A Peltier heater on which a sample rests is supplied a voltage V_p . After a delay time τ , the sample is illuminated with ultraviolet (UV) light. (b) Measured temperature T vs time t with different V_p supplied to the Peltier. (c-f) Characterization of porous PEG films using optical microscopy (top), scanning electron microscopy (middle), and histograms of pore diameter d computed from electron microscopy (bottom). Each film was prepared with $V_p = 2.5$ V and (c) $\tau = 4.5$ s, (d) $\tau = 5.5$ s, (e) $\tau = 7$ s, and (f) $\tau = 9$ s.

the salt, resulting in porous structures. Previous work has shown that the average size of these crystals can be adjusted to provide control over the average pore size in the polymer matrix, but this process provides no spatial control.^{22–28}

To begin to explore how spatial control over porosity could be achieved using salt leaching, we note that the phase diagram in Figure 2a is highly temperature sensitive. This acknowledgment was critical to generating an accurate phase diagram as the stability of phases was checked after holding them overnight at room temperature. However, this temperature dependence could provide an avenue for controlling both the size and spatial distribution of phase-separated regions. In particular, mixtures of PEGDA, water, and salt prepared at low temperature to be within the single phase region L can undergo a spinodal decomposition into L₁ and L₂ at a spinodal temperature T_s. To explore this temperature-dependent miscibility, samples were prepared with compositions in regime L and heated until spinodal decomposition was observed, providing a measure of T_s (Figure 2b). For example, a sample that was 60:5:35 PEGDA:NaCl:H₂O by weight is fully miscible at room temperature but becomes immiscible at $T_s = 32$ °C. This is important because it implies that samples can be prepared and manipulated at room temperature, and then nucleation can be initiated at a specified time, potentially

giving rise to a relatively uniform array of porogenic domains of L_1 . However, as a nucleation process, the spinodal decomposition of L into L_1 and L_2 will result in drops of L_1 whose average diameter will increase through coarsening and Ostwald ripening. Thus, to produce a well-controlled distribution of porogens, the coarsening process must be halted at a specified time point.

Prior to exploring the interaction between light and heat in salt solutions, thin films were prepared to simplify analysis and minimize the importance of thermal diffusion. Photosensitive solutions were prepared that were by weight 59.7% PEGDA, 35% water, 5% NaCl, and 0.3% 2,2-dimethoxy-2-phenylacetophenone (DMPA) to serve as a photoinitiator. Silicon wafer chips were diced to be 1 cm², chemically cleaned through rinsing with acetone and isopropanol, rendered hydrophilic upon exposure to an O2 plasma for 5 min, and acrylatefunctionalized by drop coating them with liquid (3acryloxypropyl)trimethoxysilane followed by baking at 80 °C for 2 h. After baking, the residual silane was removed by rinsing the samples with acetone and isopropanol. In order to prepare liquid films, 5 μ L of the photosensitive solution was pipetted onto the silicon chip and covered by placing a glass slide on the film. Covering the drop serves the dual purpose of flattening the film and preventing the diffusion of oxygen into the film,

which can impede photo-cross-linking in microscopic films.³¹ Acrylate functionalizing the surfaces allows the polymer to covalently attach to the silicon surface during photo-cross-linking.

In order to explore whether cross-linking the PEG network would arrest the coarsening of L₁ domains and result in a welldefined distribution of pores, we performed a series of experiments in which single-phase mixtures were prepared as thin films, heated above T_{s} , and subsequently photo-crosslinked at a fixed delay time (Figure 3a). In situ heating was achieved by placing the sample on a Peltier heater (CP13535 - CUI Inc.) on a mask aligner (MA-6 - Karl Suss). Prior to illumination, a voltage supply (1550 DC Power Supply - BK Precision) was used to supply current to the Peltier. Independent measurements of the temperature profile on the top surface of the Peltier provided a calibration of the timeand voltage-dependent temperature (Figure 3b). After a specified delay time, the sample was illuminated for 5 s with 10 mW/cm² light from a mercury lamp. In order to remove the glass slide covering the film, salt, and un-cross-linked PEGDA, the sample was then immersed in DI water for 20 min. During this process, the glass slide naturally falls off due to PEG swelling, while the PEG remains attached to the silicon surface due to covalent bonds that formed during cross-linking.³³ Further rinsing with DI water was used to ensure the complete removal of salt. While a 5 s exposure time was chosen to ensure full cross-linking, robust polymer films were observed with as little as 2 s exposure time. Exposure times less than this likely lead to cross-linking, but the films are not well adhered to the substrate so they detach during water immersion. A detailed summary of the lithographic process can be found in the Supporting Information.

Modulating the delay time τ between heating and illumination allowed us to directly observe and capture the kinetics of phase separation and coarsening. Specifically, for τ < 4.5 s, no pores were observed when the Peltier was powered with 2.5 V. Specifically, electron microscopy of a film produced with $\tau = 4$ s revealed a lack of features, indicating that no pores had formed, presumably because the film had not heated up enough to initiate spinodal decomposition (Figure S1). Under these conditions, the temperature in the film had not surpassed $T_{\rm s}$, and a homogeneous PEG film was produced after crosslinking. However, if $\tau > 4.5$ s, distinct pores were observed. Average pore size, measured using scanning electron microscopy (SEM), was found to monotonically increase with τ (Figures 3c-f). Under these conditions, the smallest average pore size was 450 \pm 66 nm with τ = 4.5 s, and the largest average pore size was found to be 2000 \pm 256 nm with $\tau = 9$ s. These results are consistent with the hypothesis that pores are dictated by the nucleation and subsequent growth of domains of L₁.

Having synthesized pores in thin films, we sought to further understand the distribution and morphology of the pores. To determine whether the pores were distributed uniformly across the thickness of the hydrogel film, we sectioned one of the hydrogel films prepared with $\tau=9$ s (Figure S2). Electron microscopy taken of the cross section of the hydrogel film revealed that the pores were predominantly localized on the top and bottom interfaces. These results suggest that heterogeneous nucleation of the domains occurs more quickly than homogeneous nucleation in the bulk. In order to determine whether thermal gradients across the film would be substantial, the time required for thermal diffusion to

equalize the temperature across the $\sim 5~\mu m$ thick film was estimated using the $\sim 10^{-7}~m^2/s$ thermal diffusivity of PEG. Since this time, which was predicted to be $\sim 300~\mu s$, is much shorter than the several second duration of the experiment, thermal gradients across the film are not expected to play a large role in determining the final structure. Careful inspection of the optical and electron microscope images revealed a lack of overlapping pores. In fact, small pores are typically absent from the vicinity of larger pores, suggesting that if they formed, they subsequently coalesced into a larger domain prior to complete cross-linking. Collectively, these observations suggest that the pores are isolated from one another and do not form an interconnected network.

Having shown that illumination can arrest phase separation and result in the formation of pores in a hydrogel film, we sought to explore the degree to which this process can be patterned. To explore this, we replaced the glass slide that covered the un-cross-linked film with a photomask. In an initial experiment to study the photopatterning of pores in hydrogels, a dark-field mask was studied that was composed of a series of circular transparent regions in a 50 nm thick aluminum film on a glass slide. Since PEGDA functions as a negative photoresist, we anticipated that combining photolithography with coordinated heating would allow us to pattern porous hydrogels (Figure 4a). In an initial experiment using the photosensitive solution formulation discussed in Figure 3, we prepared a film, heated it for $\tau=5.5$ s, and then illuminated it for 5 s. As

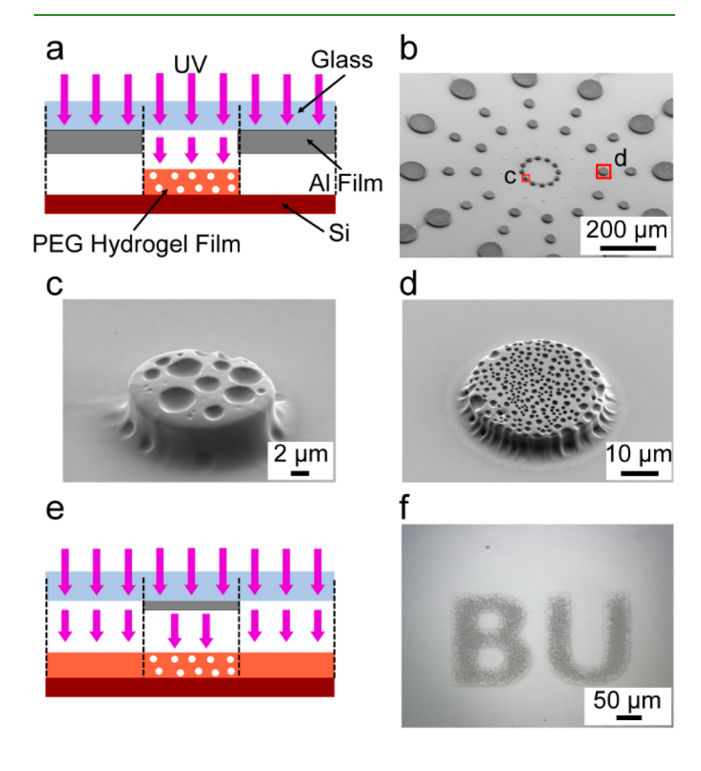


Figure 4. Patterning porous hydrogels. (a) Scheme of hydrogel patterning using a dark-field photomask. (b) SEM image showing a porous PEG sample prepared with $V_{\rm p}=2.5~{\rm V}$ and $\tau=5.5~{\rm s}$. This sample was illuminated through a mask that consisted of a series of transparent circles of varying size. Squares show the locations of magnifications depicted in (c) and (d). (e) Scheme of hydrogel patterning using a partially opaque bright-field photomask. (f) Optical microscope picture of the letters "BU" patterned on sample made by illumination through a bright-field mask composed of 20 nm thick Al. Here, $V_{\rm p}=2.5~{\rm V}$ and $\tau=3~{\rm s}$.

expected, porous hydrogel features were present in a manner that reproduced the pattern on the mask (Figures 4b-d).

While it is reassuring to prove that these photosensitive films can serve as standard photoresists, the combination of a kinetic phase separation process and light sensitivity provides further possibilities for tuning the final structure. Specifically, if a sample of phase L is heated uniformly, the nucleation and growth of L₁ domains could be arrested in a spatially dependent manner by direct light to different regions of the sample at different times. Such a process would result in a distribution of pore sizes that depend on position. While this could be realized using a spatial light modulator,³⁴ we hypothesized that an analogous process could be achieved by spatially modulating the intensity of incident light. As crosslinking occurs in an intensity-dependent fashion, regions with less intense illumination will cross-link more slowly, giving nucleation and growth of L₁ more time to occur. In order to achieve intensity modulation, we deposited aluminum films of various thicknesses on a glass slide. While aluminum films thicker than 50 nm transmit less than 0.1% of UV light, such films partially transmit UV light in a predictable manner at thicknesses <50 nm. 35,36 In this manner, we hypothesized that regions with no aluminum will promote rapid cross-linking, while regions with 20 nm aluminum will only transmit ~6% of the light, leading to a longer delay between heating and complete cross-linking (Figure 4e). In order to test this, we prepared a bright-field mask that depicted the letters "BU" as partially opaque features composed of 20 nm of aluminum. With this mask, we repeated the lithographic process with τ = 3 s before a 5 s illumination. Note that since $\tau = 3$ s is not enough time for appreciable phase separation to occur, the hydrogel film not covered by the mask formed a continuous hydrogel film, as expected (Figure 4f). However, rather than the occluded regions not cross-linking, the partial opacity of the mask allowed these regions to cross-link at a slower pace, resulting in the features being reproduced as a porous domain in an otherwise nonporous film (Figure 4f).

In order to further explore the ability of spatially modulating illumination intensity as a path to patterning pore size, we performed a series of heating and photolithography experiments using greyscale masks with a variety of attenuations on the same mask (Figure 5a, Table 1). Specifically, a photomask was prepared by depositing two orthogonal arrays of 500 μ m wide lines. As the lines were each prepared using separate lithography and deposition steps, there were four distinct thicknesses of aluminum on the sample: 0, 10, 20, and 30 nm. These thicknesses were chosen such that $\tau = 3$ s would lead to films with four distinct regions: a region with no pores corresponding to the bare slide (I - 100% transmission), a region with small pores corresponding to the 10 nm thick aluminum (II -25% transmission), a region with large pores corresponding to the 20 nm thick aluminum (III - 6% transmission), and a region that is not cross-linked corresponding the 30 nm thick aluminum (IV - ~1% transmission) (Figure 5a), highlighting the ability of this approach to generate the complete range of features in one step. After heating, illumination for 3 s, and liftoff, samples were studied using optical microscopy (Figure 5b), and the four regimes were produced as expected. The pattern fidelity was further confirmed using optical profilometry (Figure 5c).

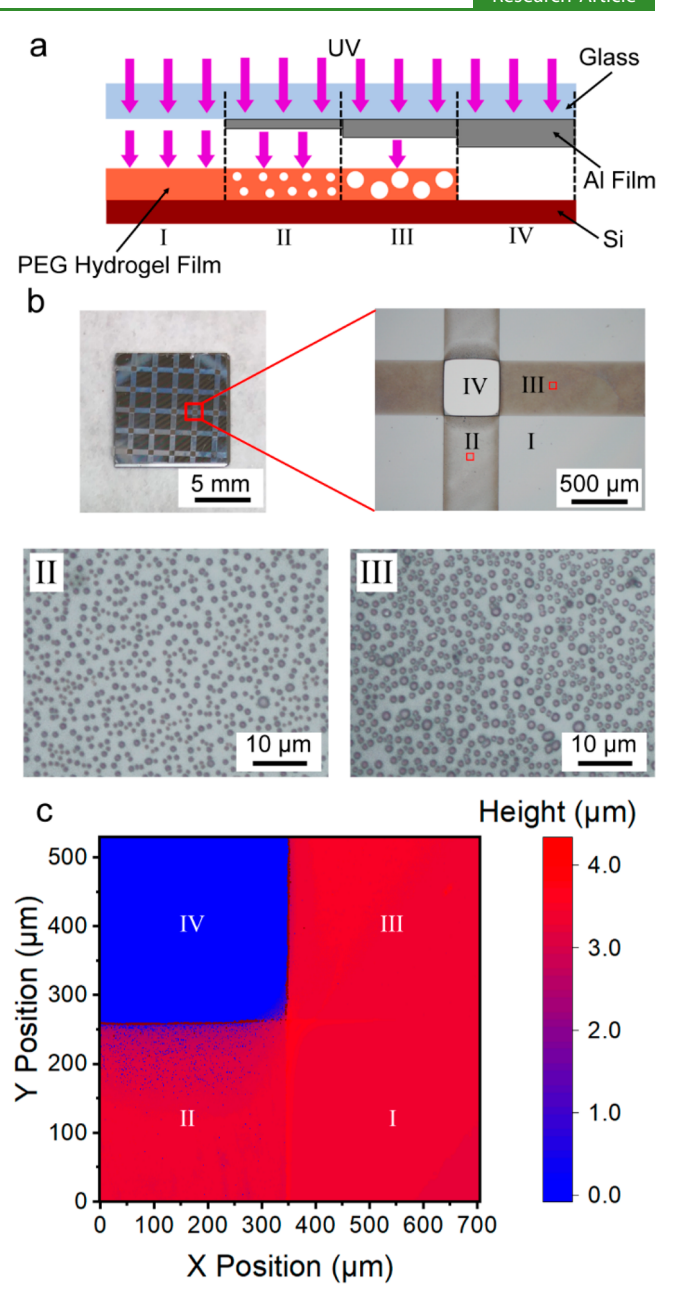


Figure 5. Pattering porosity and hydrogels. (a) Process for controlling pore sizes in a single process with a variable attenuation photomask. Four regions are identified: (I) pure hydrogel film with no pores, (II) hydrogel film with small pores, (III) hydrogel film with large pores, and (IV) region with no hydrogel. (b) Photograph and optical micrographs of sample with patterned porosity prepared with $V_{\rm p}=2.5$ V and $\tau=3$ s. Magnified images show regions II (bottom left) and III (bottom right). (c) Surface topography image from optical profilometry depicts the height difference in the four regions.

Table 1. Parameters of Variable Attenuation Experiment

| | Al thickness | transmission at 400 nm | resultant hydrogel |
|------------|-----------------|------------------------|--|
| region I | 0 nm | 100% | homogenous PEG film |
| region II | 10 nm | 25% | $0.88 \pm 0.13 \ \mu m$ diameter pores |
| region III | 20 nm | 6% | $1.1 \pm 0.2 \ \mu m$ diameter pores |
| region IV | 30 nm | 1% | no cross-linked PEG |

CONCLUSION

In summary, we have demonstrated that arresting the phase separation of mixtures of polymer, salt, and water can be leveraged to prepare hydrogel films with spatially patterned porosity. In a single lithographic step, it is possible to control the size and distribution of pores within a hydrogel as well as the presence or absence of the hydrogel itself. This is not possible using conventional salt leaching processes or any process that is based upon a pre-existing porogen. As the operating principles of this approach are general to hydrophilic polymers, this approach is expected to be applicable to a number of material systems including gels based upon other synthetic polymers or those that are naturally occurring. Finally, the scalability inherent to photolithography indicates that films can be made at large scale with control over features at the submicrometer scale. Currently, the resolution of hydrogel features produced using this method is limited to ~5 μ m by diffraction and the absence of a chemical amplification strategy for the polymer. Since the pore size is only limited by the coordination of the thermal and optical stimuli, features smaller than 400 nm may be realized, although they may become difficult to image. The maximum size of pores is expected to be governed by the thickness of the film, which was 4 to 10 μ m in the experiments presented here. Thicker films could be realized but would require one to balance homogeneous nucleation in the bulk with heterogeneous nucleation on the interfaces. It is worth highlighting that the size of the pores described herein is commensurate with pores found in other systems to promote the proliferation of human mesenchymal stem cells and even guide them down osteogenic pathways, suggesting that structures of the kind realized by this work could prove useful in tissue engineering applications.²⁰ In addition to providing an example of how top-down control can be combined with a bottom-up process for advanced nanomanufacturing,³⁷ being able to address these hierarchical length scales in a biocompatible material system presents opportunities for adopting structures made through this approach for applications in tissue engineering.

ASSOCIATED CONTENT

S Supporting Information

The Supporting Information is available free of charge on the ACS Publications website at DOI: 10.1021/acsami.8b11530.

Supplementary methods and Figures S1 and S2 (PDF)

AUTHOR INFORMATION

Corresponding Author

*E-mail: brownka@bu.edu.

ORCID

Keith A. Brown: 0000-0002-2379-2018

The authors declare no competing financial interest.

ACKNOWLEDGMENTS

This work was supported by the Air Force Office of Scientific Research (Multidisciplinary University Research Initiatives FA9550-16-1-0150) and the National Science Foundation (CMMI-1661412, Research Experiences for Undergraduates EEC-1461152, and Research Experiences for Teachers EEC-1407165). We also acknowledge support through the Boston University Photonics Center.

REFERENCES

- (1) Kirchmajer, D. M.; Gorkin, R. An Overview of the Suitability of Hydrogel-Forming Polymers for Extrusion-Based 3d-Printing. J. Mater. Chem. B 2015, 3 (20), 4105-4117.
- (2) Drury, J. L.; Mooney, D. J. Hydrogels for Tissue Engineering: Scaffold Design Variables and Applications. Biomaterials 2003, 24 (24), 4337–4351.
- (3) Nemir, S.; Hayenga, H. N.; West, J. L. Pegda Hydrogels with Patterned Elasticity: Novel Tools for the Study of Cell Response to Substrate Rigidity. Biotechnol. Bioeng. 2010, 105 (3), 636-644.
- (4) Wegst, U. G. K.; Bai, H.; Saiz, E.; Tomsia, A. P.; Ritchie, R. O. Bioinspired Structural Materials. Nat. Mater. 2015, 14 (1), 23-36.
- (5) Fratzl, P.; Weinkamer, R. Nature's Hierarchical Materials. Prog. Mater. Sci. 2007, 52 (8), 1263-1334.
- (6) Waldrop, M. M. The Chips Are Down for Moore's Law. Nature 2016, 530, 144-147.
- (7) Liu, V. A.; Bhatia, S. N. Three-Dimensional Photopatterning of Hydrogels Containing Living Cells. Biomed. Microdevices 2002, 4 (4),
- (8) Tsai, H.-Y.; Vats, K.; Yates, M. Z.; Benoit, D. S. Two-Dimensional Patterns of Poly (N-Isopropylacrylamide) Microgels to Spatially Control Fibroblast Adhesion and Temperature-Responsive Detachment. Langmuir 2013, 29 (39), 12183-12193.
- (9) Barry, R. A.; Shepherd, R. F.; Hanson, J. N.; Nuzzo, R. G.; Wiltzius, P.; Lewis, J. A. Direct-Write Assembly of 3d Hydrogel Scaffolds for Guided Cell Growth. Adv. Mater. 2009, 21 (23), 2407-
- (10) Annabi, N.; Nichol, J. W.; Zhong, X.; Ji, C.; Koshy, S.; Khademhosseini, A.; Dehghani, F. Controlling the Porosity and Microarchitecture of Hydrogels for Tissue Engineering. Tissue Eng., Part B 2010, 16 (4), 371-383.
- (11) Kim, J.; Yaszemski, M. J.; Lu, L. Three-Dimensional Porous Biodegradable Polymeric Scaffolds Fabricated with Biodegradable Hydrogel Porogens. Tissue Eng., Part C 2009, 15 (4), 583-594.
- (12) Visser, J.; Melchels, F. P.; Jeon, J. E.; Van Bussel, E. M.; Kimpton, L. S.; Byrne, H. M.; Dhert, W. J.; Dalton, P. D.; Hutmacher, D. W.; Malda, J. Reinforcement of Hydrogels Using Three-Dimensionally Printed Microfibres. Nat. Commun. 2015, 6, 6933.
- (13) Gutiérrez, M. C.; Ferrer, M. L.; del Monte, F. Ice-Templated Materials: Sophisticated Structures Exhibiting Enhanced Functionalities Obtained after Unidirectional Freezing and Ice-Segregation-Induced Self-Assembly. Chem. Mater. 2008, 20 (3), 634-648.
- (14) Bai, H.; Polini, A.; Delattre, B.; Tomsia, A. P. Thermoresponsive Composite Hydrogels with Aligned Macroporous Structure by Ice-Templated Assembly. Chem. Mater. 2013, 25 (22), 4551-4556.
- (15) Lima, E. G.; Durney, K. M.; Sirsi, S. R.; Nover, A. B.; Ateshian, G. A.; Borden, M. A.; Hung, C. T. Microbubbles as Biocompatible Porogens for Hydrogel Scaffolds. Acta Biomater. 2012, 8 (12), 4334-4341.
- (16) Chiu, Y.-C.; Larson, J. C.; Isom, A.; Brey, E. M. Generation of Porous Poly(Ethylene Glycol) Hydrogels by Salt Leaching. Tissue Eng., Part C **2009**, 16 (5), 905–912.
- (17) Mygind, T.; Stiehler, M.; Baatrup, A.; Li, H.; Zou, X.; Flyvbjerg, A.; Kassem, M.; Bünger, C. Mesenchymal Stem Cell Ingrowth and Differentiation on Coralline Hydroxyapatite Scaffolds. Biomaterials 2007, 28 (6), 1036-1047.
- (18) O'Brien, F. J.; Harley, B. A.; Yannas, I. V.; Gibson, L. J. The Effect of Pore Size on Cell Adhesion in Collagen-Gag Scaffolds. Biomaterials 2005, 26 (4), 433-441.
- (19) Zeltinger, J.; Sherwood, J. K.; Graham, D. A.; Müeller, R.; Griffith, L. G. Effect of Pore Size and Void Fraction on Cellular Adhesion, Proliferation, and Matrix Deposition. Tissue Eng. 2001, 7 (5), 557-572.
- (20) Kasten, P.; Beyen, I.; Niemeyer, P.; Luginbühl, R.; Bohner, M.; Richter, W. Porosity and Pore Size of B-Tricalcium Phosphate Scaffold Can Influence Protein Production and Osteogenic Differentiation of Human Mesenchymal Stem Cells: An in Vitro and in Vivo Study. Acta Biomater. 2008, 4 (6), 1904–1915.

- (21) Cheluget, E. L.; Gelinas, S.; Vera, J. H.; Weber, M. E. Liquid-Liquid Equilibrium of Aqueous Mixtures of Poly (Propylene Glycol) with Sodium Chloride. *J. Chem. Eng. Data* **1994**, *39* (1), 127–130.
- (22) Chiu, Y.-C.; Larson, J. C.; Isom, A., Jr; Brey, E. M. Generation of Porous Poly (Ethylene Glycol) Hydrogels by Salt Leaching. *Tissue Eng., Part C* **2010**, *16* (5), 905–912.
- (23) Nam, Y. S.; Yoon, J. J.; Park, T. G. A Novel Fabrication Method of Macroporous Biodegradable Polymer Scaffolds Using Gas Foaming Salt as a Porogen Additive. *J. Biomed. Mater. Res.* **2000**, *53* (1), 1–7.
- (24) Kim, T. G.; Chung, H. J.; Park, T. G. Macroporous and Nanofibrous Hyaluronic Acid/Collagen Hybrid Scaffold Fabricated by Concurrent Electrospinning and Deposition/Leaching of Salt Particles. *Acta Biomater.* **2008**, *4* (6), 1611–1619.
- (25) Hou, Q.; Grijpma, D. W.; Feijen, J. Porous Polymeric Structures for Tissue Engineering Prepared by a Coagulation, Compression Moulding and Salt Leaching Technique. *Biomaterials* **2003**, *24* (11), 1937–1947.
- (26) Nasri-Nasrabadi, B.; Mehrasa, M.; Rafienia, M.; Bonakdar, S.; Behzad, T.; Gavanji, S. Porous Starch/Cellulose Nanofibers Composite Prepared by Salt Leaching Technique for Tissue Engineering. *Carbohydr. Polym.* **2014**, *108*, 232–238.
- (27) Guan, J.; Fujimoto, K. L.; Sacks, M. S.; Wagner, W. R. Preparation and Characterization of Highly Porous, Biodegradable Polyurethane Scaffolds for Soft Tissue Applications. *Biomaterials* **2005**, *26* (18), 3961–3971.
- (28) Heijkants, R.; Van Tienen, T.; De Groot, J.; Pennings, A.; Buma, P.; Veth, R.; Schouten, A. Preparation of a Polyurethane Scaffold for Tissue Engineering Made by a Combination of Salt Leaching and Freeze-Drying of Dioxane. *J. Mater. Sci.* **2006**, *41* (8), 2423–2428.
- (29) Huang, Z.; Su, M.; Yang, Q.; Li, Z.; Chen, S.; Li, Y.; Zhou, X.; Li, F.; Song, Y. A General Patterning Approach by Manipulating the Evolution of Two-Dimensional Liquid Foams. *Nat. Commun.* **2017**, *8*, 14110.
- (30) Zhang, Z.; Wang, Z.; He, S.; Wang, C.; Jin, M.; Yin, Y. Redox Reaction Induced Ostwald Ripening for Size-and Shape-Focusing of Palladium Nanocrystals. *Chem. Sci.* **2015**, *6* (9), 5197–5203.
- (31) Lee, T.; Guymon, C.; Jönsson, E. S.; Hoyle, C. E. The Effect of Monomer Structure on Oxygen Inhibition of (Meth) Acrylates Photopolymerization. *Polymer* **2004**, *45* (18), 6155–6162.
- (32) Millet, L. J.; Corbin, E. A.; Free, R.; Park, K.; Kong, H.; King, W. P.; Bashir, R. Characterization of Mass and Swelling of Hydrogel Microstructures Using Mems Resonant Mass Sensor Arrays. *Small* **2012**, *8* (16), 2555–2562.
- (33) Choi, J.; Bischof, J. C. Review of Biomaterial Thermal Property Measurements in the Cryogenic Regime and Their Use for Prediction of Equilibrium and Non-Equilibrium Freezing Applications in Cryobiology. *Cryobiology* **2010**, *60* (1), 52–70.
- (34) Liao, X.; Brown, K. A.; Schmucker, A. L.; Liu, G.; He, S.; Shim, W.; Mirkin, C. A. Desktop Nanofabrication with Massively Multiplexed Beam Pen Lithography. *Nat. Commun.* **2013**, *4*, 2103.
- (35) Hass, G.; Waylonis, J. Optical Constants and Reflectance and Transmittance of Evaporated Aluminum in the Visible and Ultraviolet. J. Opt. Soc. Am. 1961, 51 (7), 719–722.
- (36) Ehrenreich, H.; Philipp, H.; Segall, B. Optical Properties of Aluminum. *Phys. Rev.* **1963**, *132* (5), 1918.
- (37) Isaacoff, B. P.; Brown, K. A. Progress in Top-Down Control of Bottom-up Assembly. *Nano Lett.* **2017**, *17* (11), 6508–6510.